Hydrodynamic Interaction Between a Platelet and an Erythrocyte: Effect of Erythrocyte Deformability, Dynamics, and Wall Proximity

Koohyar Vahidkhah
Department of Mechanical and Aerospace Engineering,
Rutgers,
The State University of New Jersey,
Piscataway, NJ 08854

Scott L. Diamond
Department of Chemical and Biomolecular Engineering,
University of Pennsylvania,
Philadelphia, PA 19104

Prosenjit Bagchi[1]
Department of Mechanical and Aerospace Engineering,
Rutgers,
The State University of New Jersey,
Piscataway, NJ 08854
e-mail: pbagchi@jove.rutgers.edu

We present three-dimensional numerical simulations of hydrodynamic interaction between a red blood cell (RBC) and a platelet in a wall-bounded shear flow. The dynamics and large deformation of the RBC are fully resolved in the simulations using a front-tracking method. The objective is to quantify the influence of tank treading and tumbling dynamics of the RBC, and the presence of a bounding wall on the deflection of platelet trajectories. We observe two types of interaction: A crossing event in which the platelet comes in close proximity to the RBC, rolls over it, and continues to move in the same direction; and a turning event in which the platelet turns away before coming close to the RBC. The crossing events occur when the initial lateral separation between the cells is above a critical separation, and the turning events occur when it is below the critical separation. The critical lateral separation is found to be higher during the tumbling motion than that during the tank treading. When the RBC is flowing closer to the wall than the platelet, the critical separation increases by several fold, implying the turning events have higher probability to occur than the crossing events. On the contrary, if the platelet is flowing closer to the wall than the RBC, the critical separation decreases by several folds, implying the crossing events are likely to occur. Based on the numerical results, we propose a mechanism of continual platelet drift from the RBC-rich region of the vessel towards the wall by a succession of turning and crossing events. The trajectory deflection in the crossing events is found to depend nonmonotonically on the initial lateral separation, unlike the monotonic trend observed in tracer particle deflection and in deformable sphere-sphere collision. This nonmonotonic trend is shown to be a consequence of the deformation of the RBC caused by the platelet upon collision. An estimation of the platelet diffusion coefficient yields values that are similar to those reported in experiments and computer simulations with multicellular suspension. [DOI: 10.1115/1.4023522]

1 Introduction

Blood is a multiphase fluid composed of red blood cells (RBC), white blood cells, and platelets suspended in plasma. Platelets play a critical physiological role in the formation of hemostatic plug at vascular walls, and in the growth of thrombosis under pathological conditions [1–3]. Experiments with whole blood as well as ghost cell suspension showed an elevated platelet concentration near the wall [4–11]. This phenomenon of platelet margination (also known as lateral drift) serves to enhance hemostatic or thrombotic events as it increases the number of platelets available for capture near the wall. Margination of the platelets toward the vascular wall is critically dependent on their interaction with the red blood cells which has been illustrated in several experiments [12–16]. These studies have demonstrated that the near-wall excess was absent in platelet-rich plasma and in suspension of hardened red blood cells [17,18], and only occurred when the hematocrit was above a threshold level beyond which the accumulation was observed to increase with increasing hematocrit [10]. Several possible mechanisms are thought to underlie the margination process. The first is the volume exclusion process whereby the platelets are pushed towards the wall by a lateral motion of the RBC towards the center of the vessel [6,9]. The lateral migration of the RBC in a shear flow arises due to its deformability [19]. The second mechanism is the spatially dependent collision rate [5,20]. In a shearing flow, the continuous collision between the RBC and platelets results in significantly higher shear-induced diffusion of the platelets than the Brownian diffusion [21–23]. Since the RBC migration causes a concentration gradient, a net flux of platelets occurs from a region of higher collision rate to a region of lower collision rate [20]. Also, the RBC is sterically excluded from the plasma layer nearest the wall. If platelets entering the plasma layer have difficulty crossing back into the bulk flow, an accumulation of platelets can occur.

The above mechanisms are, however, not complete as they do not consider certain details of the suspension. For example, the volume exclusion model is incompatible with the fact that the RBC migration occurs faster than the platelet margination [20]. The collision model is also incomplete since the RBC concentration gradient occurs over a small length [24]. Also neglected in the models are the effect of the finite size of RBC and platelet as noted in [25,26], the differences in their shapes, and the different dynamical behavior of the RBC, namely, the tank-treading and tumbling, observed under different shear rates [27–31]. It is also ambiguous which of these mechanisms prevail under specific conditions of hematocrit, shear rate, or shear rate gradients. Identification of these mechanisms through experimental observation in a dense multicomponent suspension is a very difficult task. High-fidelity computer simulations which model blood as a suspension

[1]Corresponding author.

Contributed by the Bioengineering Division of ASME for publication in the Journal of Biomechanical Engineering. Manuscript received July 9, 2012; final manuscript received January 17, 2013; accepted manuscript posted January 29, 2013; published online April 24, 2013. Assoc. Editor: Jeffrey W. Holmes.

of finite-size particles provide an alternative approach for verification of these mechanisms as well as obtaining further insights of the margination process. In the following we discuss a few of the computer simulation studies. AlMomani et al. [32] simulated RBC/platelet interaction in two dimensions by modeling the RBC as elastic particles. In addition to reproducing several experimental observations, such as the increasing effect of hematocrit on platelet margination, AlMomani et al. mentioned that the margination process seemed to occur due to the fluctuating hydrodynamic stresses that the RBCs imparted on the platelets, rather than the direct collision or volume exclusion. Crowl and Fogelson [33,34] employed a two-dimensional immersed boundary-lattice Boltzmann method, and found that the platelet diffusivity was radially dependent, and that the enhanced diffusivity in the core of the vessel along with the volume exclusion could partly explain platelet margination. Moreover, they proposed an additional drift mechanism that was localized at the edge of the RBC-depleted layer. Zhao and Shaqfeh [35] and Zhao et al. [36] performed the first fully resolved three-dimensional simulations of RBC/platelet suspension using a spectral boundary integral method and demonstrated that the platelet margination was a shear-induced diffusional process in which the wall normal velocity fluctuations propelled the platelets toward the wall.

The aforementioned computer simulations have provided a wealth of understanding on the collective or averaged motion of the platelets. Such collective motion arises from the interaction between a RBC and a nearby platelet. Hence, important knowledge can be obtained also by looking at such pairwise collisions [37]. In particular, the role of the RBC dynamics on the deflection of individual platelet trajectory can be quantified without the "noise" generated by other cells. It is well known that an isolated RBC in shear flow exhibits two types of dynamics: A tank-treading motion in which the cell behaves like a fluid droplet and orients at a fixed angle with the flow direction while the interior liquid (hemoglobin) and the cell membrane make a rotary motion, and a tumbling motion in which the cell makes a rigid bodylike flipping motion [27–31]. The question of how these two different dynamics affect the platelet trajectory has not been addressed in the literature, although prior experiments and simulations suggested an increasingly higher value of the platelet diffusivity with decreasing RBC deformability [18,36]. The importance of understanding individual pairwise collision is aptly emphasized in a recent theoretical work in which the platelet adhesion was shown to be controlled by rebounding collisions with the near-wall RBCs and the finite size of the platelets [25,26]. It is also unknown whether the presence of a bounding wall changes the nature of the pairwise interaction. By simulating platelet-platelet interaction in three dimensions, Mody and King [38,39] demonstrated that the near-wall collision frequency was significantly greater than the one far from the wall. Similar work on the near-wall RBC/platelet interaction is lacking.

In this study we present three-dimensional numerical simulations of the hydrodynamic interaction between a platelet and a red blood cell in a wall-bounded linear shear flow mimicking a parallel-plate flow chamber. The dynamics and the large deformation of the RBC are fully resolved in the simulations. We find that the pairwise interaction results in two different types of platelet trajectory: turning and crossing. The dynamics of the RBC (tank treading versus tumbling) and the wall proximity are shown to have a significant influence on the turning and crossing events. Our results tend to suggest that the turning and crossing events, when they occur in succession, serve as an effective mechanism for continual anisotropic dispersal of the platelets from the RBC-rich region of the vessel towards the wall.

2 Methodology

Hydrodynamic interaction between an erythrocyte and a platelet is simulated in three dimensions using a front-tracking/immersed boundary method [40,41]. Description of the numerical method and its validation are presented in prior publications [42–44]. The RBC/platelet pair is suspended in a linear shear flow between two parallel plates that are 35 μm apart (Fig. 1). The flow domain is a rectangular box that is periodic in x and z directions, x being the flow direction, y is the direction of the velocity gradient, and z is the direction of the vorticity. The box lengths in the x and z directions are 35 and 18 μm, respectively. The no-slip condition is applied on the top and bottom plates. The initial location of the RBC and platelet centers-of-mass with respect to the bottom wall are denoted by Y_C and Y_{PLT}, respectively, and the difference $Y_{PLT} - Y_C$ is denoted by ΔY_0. Erythrocytes are modeled as liquid-filled elastic capsules of biconcave resting shapes of end-to-end distance of 7.8 μm, surface area 134.1 μm^2 and volume 94.1 μm^8, respectively. The biconcave shape is prescribed as:

$$x = R\eta, \quad y = \frac{R}{2}\sqrt{1-r^2}(C_0 + C_2 r^2 + C_4 r^4), \quad z = R\zeta \qquad (1)$$

where $\eta^2 + \zeta^2 = r^2$ and R is adjusted to control the cell volume, and the coefficients C_0, C_2, and C_4 are taken to be 0.207, 2.003, and -1.123, respectively [45]. The platelets are modeled as nearly rigid oblate capsules of 3.6 μm end-to-end distance and 1.4 μm thickness [45]. The interior and suspending fluids are assumed to be incompressible and Newtonian. The cell membrane is represented as a zero-thickness elastic membrane, and assumed to possess the resistance against shear deformation, area dilatation, and bending. The first two types of deformation are modeled using a strain energy function

$$W = \frac{B'}{4}\left(\frac{1}{2}I_1^2 + I_1 - I_2\right) + \frac{C'}{8}I_2^2 \qquad (2)$$

where B' and C' are physical constants, and I_1 and I_2 are the strain invariants defined as $I_1 = \epsilon_1^2 + \epsilon_2^2 - 2$, and $I_2 = \epsilon_1^2\epsilon_2^2 - 1$, where ϵ_1 and ϵ_2 are the principal stretch ratios [46]. The constants are related to the membrane shear elastic modulus G_s and the area

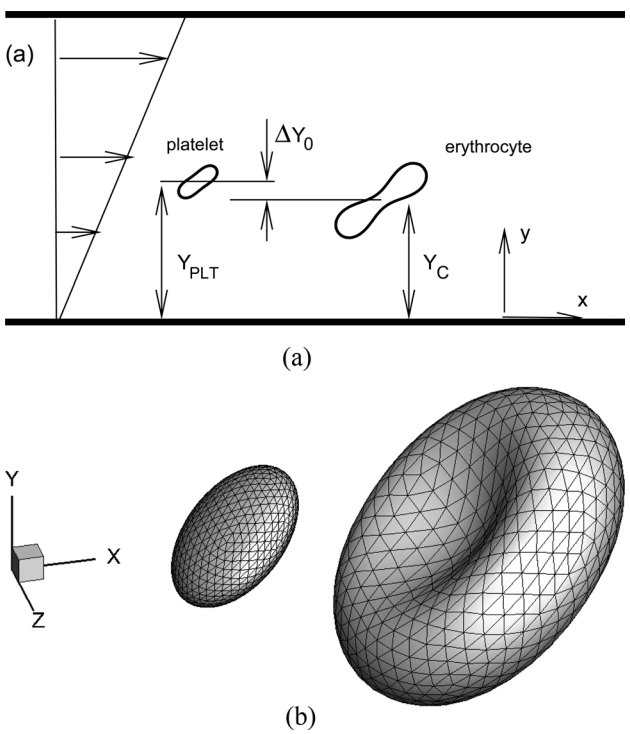

Fig. 1 (*a*) Schematic of the computation geometry. (*b*) Discretization of the cell surface. The actual number of triangles (20,480) is much higher than what is shown. The results will be plotted relative to the RBC center-of-mass.

dilatation modulus K_s as $B' = 2G_s$, $C' = 2CG_s$, and $K_s = 2G_s(1+C)$ for small deformation. The area dilatation is restricted by a large value of C as in case of a red blood cell for which the surface is nearly area incompressible. The corresponding elastic force in the membrane is obtained as:

$$\mathbf{f}_e = -\partial W / \partial \mathbf{v} \tag{3}$$

where $\mathbf{v}$ is the displacement of a Lagrangian point on the cell surface. The bending resistance is modeled following Helfrich's formulation of the surface force density

$$\mathbf{f}_b = E_b\left[(2\kappa + c_o)\left(2\kappa^2 - 2\kappa_g - c_o\kappa\right) + 2\Delta_{\mathrm{LB}}\kappa\right]\mathbf{n} \tag{4}$$

where E_b is the bending modulus associated with the mean curvature κ, κ_g is the Gaussian curvature, $\mathbf{n}$ is the surface normal, c_o is the spontaneous curvature, and Δ_{LB} is the Laplace-Beltrami operator [47,48]. The fluid motion is governed by the continuity and Navier-Stokes equations

$$\nabla \cdot \mathbf{u} = 0 \tag{5}$$

$$\rho\left[\frac{\partial \mathbf{u}}{\partial t} + \mathbf{u}\cdot\nabla\mathbf{u}\right] = -\nabla p + \nabla\cdot\mu\left[\nabla\mathbf{u} + (\nabla\mathbf{u})^T\right] \tag{6}$$

The membrane forces are coupled to the bulk flow by adding a source term

$$\mathbf{F} = \int_S (\mathbf{f}_e + \mathbf{f}_b)\delta(\mathbf{x} - \mathbf{x}')\mathrm{d}\mathbf{x}' \tag{7}$$

to the right-hand side of (6), where δ is the three-dimensional Dirac-delta function, and $\mathbf{x}'$ is a Lagrangian point on the cell surface [40,41]. The cells are advected by advecting the marker points on the membrane as $\mathrm{d}\mathbf{x}'/\mathrm{d}t = \mathbf{u}_m$, where the membrane velocity $\mathbf{u}_m$ is obtained by interpolating the local fluid velocity $\mathbf{u}$ using the delta function. The Navier-Stokes equations are solved on a fixed rectangular grid employing 225, 224, and 112 mesh points in the x, y, and z directions, respectively. A combined second-order finite difference scheme and a Fourier transform are used for the spatial discretization, and a second-order time-split scheme is used for the temporal discretization of the Navier-Stokes equations. The erythrocyte and platelet surfaces are discretized using 20,480 triangular elements (Fig. 1). The elastic force $\mathbf{f}_c$ is computed from (2) and (3) using a finite element method [49]. The curvatures are calculated by fitting a quadratic surface locally on the capsule surface and using a least-square method to find the coefficients. Further details on the methodology can be found in [42–44].

In the simulations, the governing equations are solved in dimensionless form. We use the radius of the equivalent sphere $a_o = (3V/4\pi)^{1/3}$ as the length scale, where V is the cell volume, and the inverse shear rate $\dot{\gamma}^{-1}$ as the time scale to make the equations dimensionless. The dimensionless time is denoted by $t^* = t\dot{\gamma}$. The major control parameter in dimensionless form is the capillary number of the erythrocyte defined as $\mathrm{Ca} = \dot{\gamma}\mu_o a_o / B'$, where μ_o is the dynamic viscosity of the suspending medium. The capillary number represents the ratio of the viscous (fluid) force to the elastic force. We consider two values of Ca, 0.03 and 0.7. Considering the mechanical properties of the RBC membrane reported in the literature, $G_s \approx 10^{-3}$ dyn/cm, and $a_o \sim 3\,\mu$m, the two values of Ca considered here correspond to shear rates of about 50 and 1000 1/s. For the lower value, the fluid force is weaker than the elastic force. Then the RBC is nearly rigidified and performs the tumbling motion. For the higher value of Ca, the elastic force is weaker, and a large deformation of the RBC occurs whereby it loses the initial biconcave shape. In this case, the RBC performs the tank-treading motion. The RBC internal viscosity is assumed to be the same as the suspending medium viscosity μ_o. It should be noted that for normal RBC suspended in plasma, the internal to external viscosity ratio is about 5. At this high viscosity ratio, a steady tank-treading motion was not experimentally observed even at high capillary numbers. Our recent work on single RBC dynamics using the same numerical methodology used here agreed with this known result [50]. Then, the tank-treading motion at $\mathrm{Ca} = 0.7$ is observed in our simulation due to the higher suspending medium viscosity, and zero membrane viscosity. However, tank-treading at higher viscosity ratio can occur in a dense RBC suspension [51,52]. The other relevant parameters are the initial lateral separation (along y direction) of the centers-of-mass of the RBC and platelet, $\Delta Y_o = Y_{\mathrm{PLT}} - Y_{\mathrm{C}}$. Additional geometric parameters are introduced later as needed. The capillary number for the platelet, defined in the similar way as above, is kept fixed at 0.002 so that it behaves as a nearly rigid particle. The dimensionless bending rigidity $E_b^* = E_b / a_o^2 B'$ is set to 0.01. The global and local surface area dilatation is ensured to be less than 0.5%, as the cell membranes are nearly area incompressible. The effect of inertia is small as the Reynolds number $\mathrm{Re} = \rho a_o^2 \dot{\gamma} / \mu_o \approx 10^{-2}$. All results are presented relative to the RBC center-of-mass. It may be noted that we neglected the presence of glycocalyx on the vessel wall which may influence the radial migration of the cells near the wall, see, e.g., [53].

3 Results

In the following, the first two sections present the results when the RBC/platelet pair is located away from a wall. For such a configuration, the RBC is initially placed at the centerline of the channel, which is about 18 μm from the wall. We have separately verified that the dynamics of RBC does not show any appreciable difference by taking a bigger channel height ($\gtrsim$35 μm) and placing the RBC even further away from the wall. RBC deformation, inclination angle, and dynamics remain nearly unchanged. Furthermore, the wall effect (e.g., wall-induced lateral velocity of a deformable drop) is known to decrease as inverse square of the distance from the wall. Thus, the wall effect is negligible for such a configuration. The effect of wall proximity is considered in the third section.

3.1 Turning and Crossing Trajectories. First we consider the RBC/platelet interaction in presence of a tank-treading RBC ($\mathrm{Ca} = 0.7$). Figure 2 shows the sequence of the RBC/platelet interaction obtained from our simulations for such a run. As evident from the figure, during the tank-treading motion the biconcave resting shape of the RBC is lost, and it assumes an elongated oblate shape aligning at an angle with the flow direction, while the cell membrane and the interior hemoglobin make a rotary motion. A marker point is tracked along the RBC membrane to illustrate the tank treading in the figure. Such a motion is also accompanied by a small amount of time-dependent deformation characterized by periodic stretching and compression of the RBC, and a small angular oscillation, as shown in the figure and also observed elsewhere [29–31]. In comparison, being nearly rigid the platelet undergoes a flipping motion in agreement with Jeffery's theory for rigid ellipsoids [54]. Two different types of interactions, a *crossing* and a *turning*, are observed depending on the initial lateral separation ΔY_o of the platelet center-of-mass relative to the RBC. In a *crossing*-type interaction (Fig. 2(*a*)), the platelet comes close to the RBC, rolls over it, and continues to move in the same direction. During the process, the rigid platelet causes some amount of deformation of the relatively flexible RBC as visible in the figure. After the interaction, the lateral separation ΔY is higher than the initial offset ΔY_o. In a suspension of many particles, such increased separation due to binary interaction leads to the shear-induced diffusion. In a *turning*-type interaction (Fig. 2(*b*)), the platelet first approaches the RBC, but then reverses its motion and turns away without coming close to the RBC. The turning event illustrates a long-range interaction as it occurs when the platelet is several diameters away from the RBC.

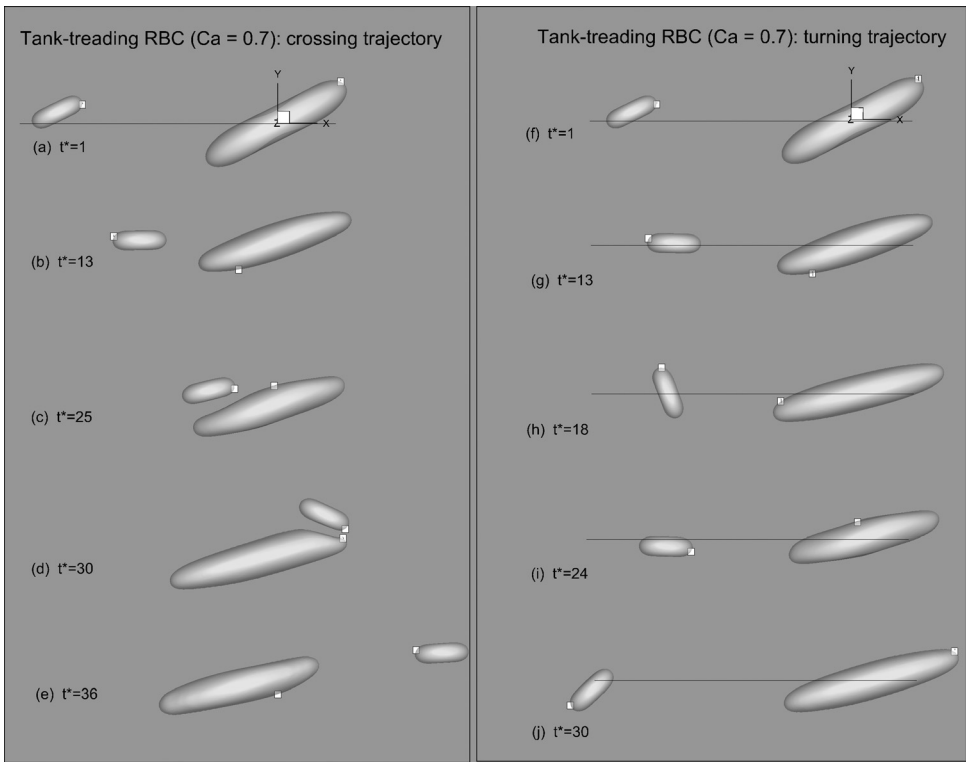

Fig. 2 Simulation results showing the sequence of two different types of interactions in presence of a tank-treading RBC. Here Ca = 0.7 corresponding to $\dot{\gamma} \approx 1000$ 1/s. (*a*)–(*e*) Crossing-type interaction. (*f*)–(*j*) Turning interaction. Marker points are shown in the cell surface which rotates along the surface indicating a tank-treading motion of the RBC. $t^* = 30$ corresponds to a 30 ms interaction.

The trajectory of the platelet relative to the tank-treading RBC is shown in Fig. 3 for several runs in which the initial lateral separation ΔY_o is varied. It is observed that the crossing events occur for $\Delta Y_o \geq 0.7\ \mu$m, and the turning events occur for $\Delta Y_o \leq 0.56\ \mu$m. The results suggest that there is a critical separation $\Delta Y_{o,\mathrm{crit}}$; the turning events occur when $\Delta Y_o \leq \Delta Y_{o,\mathrm{crit}}$, and the crossing events occur when $\Delta Y_o \geq \Delta Y_{o,\mathrm{crit}}$.

In Figs. 2 and 3, the initial orientation of the RBC and platelet major axis with respect to the flow direction was set to $\pi/4$. For nonspherical particles, as is the case, the relative orientation at the time of collision is expected to affect their trajectory. Hence, we explore the effect of the initial relative orientation $\Delta\theta_o = \theta_{o,\mathrm{RBC}} - \theta_{o,\mathrm{PLT}}$ between the platelet and RBC major axes,

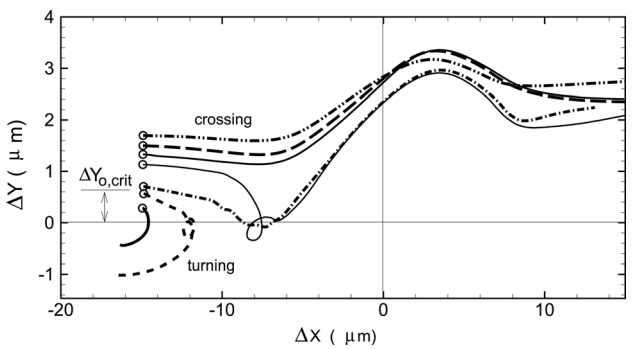

Fig. 3 The trajectory of the platelet center-of-mass relative to a tank-treading RBC. The initial location of the platelet is marked by ○ here and hereafter. Results from seven simulations are presented with different initial lateral separation ΔY_o. The turning trajectory is observed for $\Delta Y_o \leq 0.56\ \mu$m, and the crossing trajectory is observed for $\Delta Y_o \geq 0.7\ \mu$m.

where $\theta_{o,\mathrm{RBC}}$ and $\theta_{o,\mathrm{PLT}}$ are the initial orientation of the RBC and platelet, respectively. It should be mentioned that the tank-treading RBC considered here aligns at a mean angle of approximately 17 deg with the flow direction which is independent of the initial orientation of the RBC at the start of the simulations. In other words, the RBC has a preferred orientation in the tank-treading motion [29–31]. In contrast, the platelet has no preferred orientation due to its flipping motion, although it tends to spend longer in the horizontal orientation [50]. Hence, different values of $\Delta\theta_o$ were considered. For each $\Delta\theta_o$, a range of initial separation ΔY_o is considered. For each run, the crossing or turning events are noted. These results are shown in a phase plot in the $\Delta\theta_o - \Delta Y_o$ plane in Fig. 4(*a*). As the figure demonstrates, a crossing event is observed for all values of $\Delta\theta_o$ if $\Delta Y_o > 0.7\ \mu$m. For $\Delta Y_o < 0.6\ \mu$m, a turning trajectory is observed regardless of the value of $\Delta\theta_o$. The value of the critical separation $\Delta Y_{o,\mathrm{crit}}$ is found to lie between 0.6 and 0.7 μm for the tank-treading RBC. The occurrence of the turning or crossing event is independent of the relative orientation of the RBC/platelet pair, but depends on the initial separation ΔY_o. However, the actual trajectory is dependent on $\Delta\theta_o$. Figures 4(*b*) and 4(*c*) show representative platelet trajectories for crossing and turning events, respectively, for different values of $\Delta\theta_o$. As these figures demonstrate, the exact trajectory is indeed dependent on $\Delta\theta_o$, but the occurrence of the turning or crossing event is not.

Another important observation in Figs. 4(*b*) and 4(*c*) is the wide variability of the platelet trajectory over the range of $\Delta\theta_o$ for a fixed ΔY_o. For the turning trajectories shown in Fig. 4(*b*) for four different values of $\Delta\theta_o$, the platelets are deflected in to different regions of the flow. This happens because the tank-treading RBC undergoes a small-amplitude shape and angular oscillation that introduces a weak time dependency of the streamlines. This result is remarkable as it shows how the platelets can be dispersed by the RBC via a long-range interaction. A wide variability of the

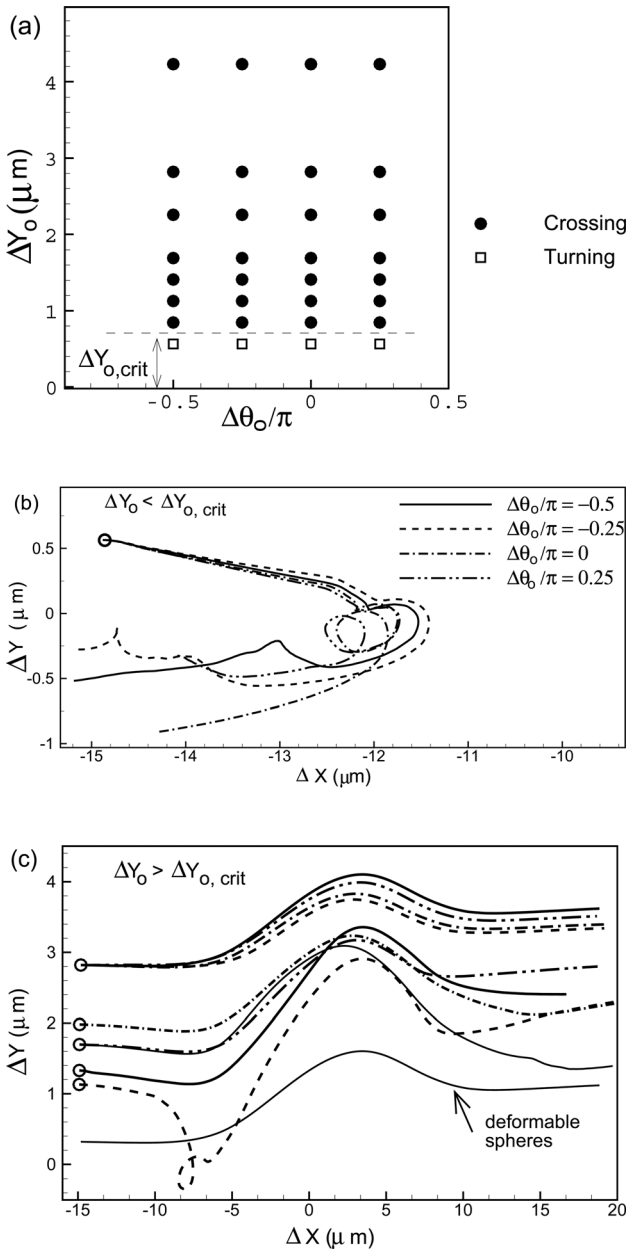

Fig. 4 Effect of initial relative orientation $\Delta\theta_o$ on turning and crossing events in presence of a tank-treading RBC. (*a*) Phase plot in $\Delta\theta_o - \Delta Y_o$ plane. (*b*) and (*c*) sample trajectories obtained with different $\Delta\theta_o$ for turning and crossing events, respectively. The wide variability of the platelet trajectory is illustrated in (*c*) that is absent in deformable sphere-sphere interaction.

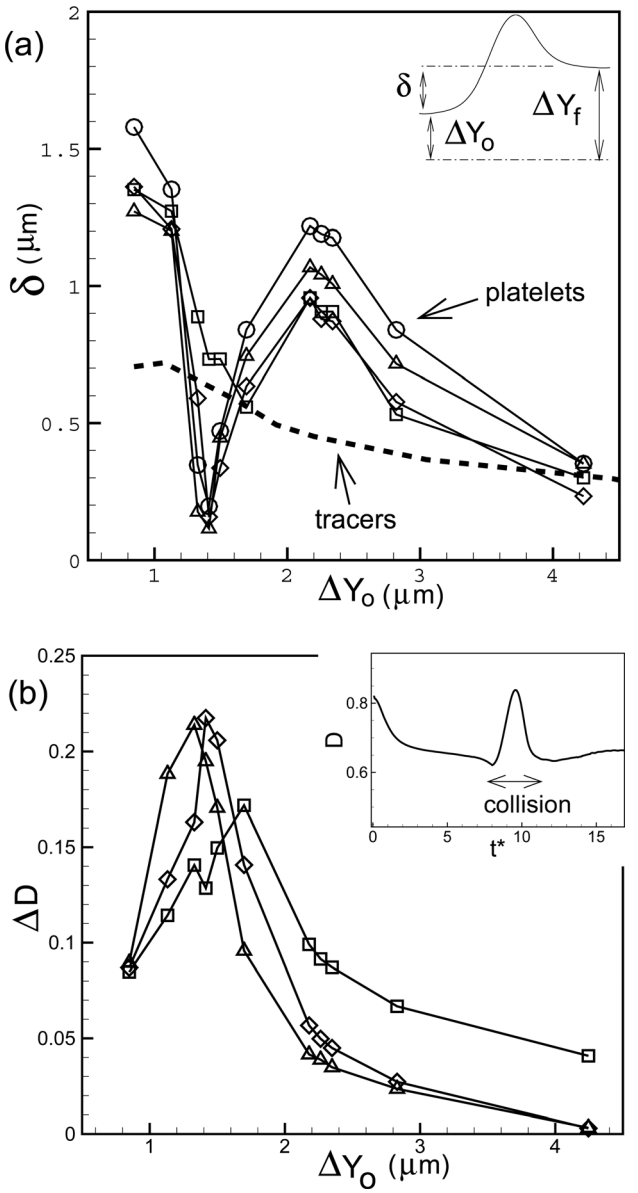

Fig. 5 (*a*) Deflection δ of platelet trajectory for the tank-treading RBC as a function of ΔY_o and for different values of $\Delta\theta_o = \pi/4$ (Δ), 0 (◇), $-\pi/4$ (□), $-\pi/2$ (○). The dashed line represents the deflection of passive tracers. (*b*) The change in RBC deformation index ΔD upon collision with the platelet is plotted. Inset shows the time-dependent deformation index D increases during the collision.

platelet trajectory can also happen during the crossing events as shown in Fig. 4(*c*). Here a small change in the initial separation ΔY_o can lead to a wide variation in the post-interaction separation. It is also evident in Fig. 4(*c*) that a monotonic change in ΔY_o does not cause a monotonic change in the post-interaction separation. In other words, a platelet released at a smaller ΔY_o can end up at a larger post-interaction separation, whereas a platelet released at a larger ΔY_o can end up at a smaller separation. In some simulations we observe that the post-interaction separation does not reach a steady value even when the platelet has moved away from the RBC. It is interesting to compare these results with that of deformable sphere-sphere interaction for which a sample trajectory obtained from our simulations is shown in Fig. 4(*c*). For the sphere-sphere interaction, a crossing event always leads to an increased lateral separation, and a monotonic change in ΔY_o leads to a monotonic change in the post-interaction separation [55,56], unlike what is seen here for the RBC/platelet interaction. Thus the wide variability of the trajectories observed in the RBC/platelet interaction is absent in the sphere-sphere interaction, and is essentially due to the nonspherical shapes of these cells. This observation also suggests that the shear-induced diffusion process in the RBC/platelet suspension is more complex with a significantly greater amount of anisotropic mixing than that in a spherical particle suspension.

For the crossing-type interactions for which the post-interaction lateral separation ΔY_f reaches a steady value, the deflection of the platelet trajectory can be quantified as $\delta = \Delta Y_f - \Delta Y_o$, which can be considered as an indirect measure of the platelet drift arising from the crossing-type collisions [see inset of Fig. 5(*a*) for definition]. Figure 5(*a*) shows δ as a function of ΔY_o for different $\Delta\theta_o$ for the tank-treading RBC. For a deformable sphere-sphere

collision, δ continually decreases with increasing ΔY_o as noted earlier. While this trend is generally observed for the RBC/platelet interaction, the data in Fig. 5(*a*) shows a more complex trend that δ has a nonmonotonic dependency on ΔY_o with a local minimum at $\Delta Y_o \sim 1.3 - 1.8\ \mu$m. While the actual value of δ is dependent on $\Delta\theta_o$ resulting in the scatter of the data, all curves for different $\Delta\theta_o$ show the similar qualitative trend.

It should be mentioned that the above results for δ are obtained for the RBC/platelet pair located away from a wall. The positive (or negative) values of δ in the figure do not imply whether the platelet move away from (or toward) the wall. It simply means the amount of additional lateral (or cross-stream) displacement of the platelet upon interaction.

The nonmonotonic variation of δ can be understood by recalling that during the crossing-type interactions, the platelet can cause a deformation of the RBC as observed in Fig. 2(*a*). Analysis of the RBC shape suggests that the platelet causes a dimple upon collision near the RBC center, and thereby it is drawn closer to the cell resulting a reduced value of ΔY_f. The time-dependent RBC deformation during the collision process can be quantified by the Taylor deformation index $D = (L - B)/(L + B)$, where L and B are, respectively, the longest and shortest end-to-end lengths of the RBC in the shear plane passing through the center-of-mass. The deformation index which is plotted in the inset of Fig. 5(*b*) as a function of time shows an increase at the time of collision. The change in the deformation index ΔD, defined as the difference in the maximum value of D reached during the collision and the value of D before the collision is shown in Fig. 5(*b*) as a function of ΔY_o. A comparison of Figs. 5(*a*) and 5(*b*) readily suggests that the minimum δ occurs at the same ΔY_o at which ΔD is maximum, implying that the nonmonotonic nature of the platelet deflection δ is due to the collision-induced deformation of the RBC. For larger separation, the platelet does not come close enough to impart any deformation, and its deflection follows that of the streamlines. Hence, in this range, δ continually decreases with increasing ΔY_o since the streamlines away from the RBC deflect less than those near the RBC.

We have also simulated transport of passive tracers as massless point particles in presence of the tank-treading RBC. The deflection of the tracer particles is plotted in Fig. 5(*a*) which shows a continuous decrease with increasing ΔY_o, unlike the nonmonotonic trend observed for the platelet. Except the local minimum near $\Delta Y_o \sim 1.3 - 1.8\ \mu$m, the platelet deflection is generally higher than the tracer particle deflection. The peak deflections of the platelet at $\Delta Y_o \sim 0.8$ and $2.2\ \mu$m are nearly twofold higher than that of the tracer particle.

3.2 Tank Treading Versus Tumbling RBC. Next we consider the RBC/platelet interaction when the RBC is in tumbling motion. As in case of a tank-treading RBC, here also we observe two types of interaction, crossing and turning. However, it is observed that the critical separation $\Delta Y_{o,\mathrm{crit}}$ is higher for the tumbling RBC. Thus, the turning event occurs more often when the RBC is tumbling than when it is tank treading. For the same values of $\Delta Y_{o,\mathrm{crit}}$ near the critical value, a crossing trajectory is observed when the RBC is tank treading, but a turning trajectory is observed when it is tumbling. In addition to the turning and crossing, a third type of interaction is observed in presence of the tumbling RBC. Here the platelet first approaches the RBC in a way that resembles a crossing interaction. But as it gets closer, it appears to "ride" on the RBC with its major axis staying parallel to that of the RBC. After about a half tumble of the RBC, the platelet starts to move away in the manner of a turning event. Note that the riding event is a close-range interaction unlike a turning event.

In presence of the tumbling RBC, the initial relative orientation $\Delta\theta_o$ makes a greater effect on the platelet motion in two different ways. First, for a given initial separation ΔY_o, it is possible to have three different types of interaction, namely, crossing, turning, and riding, depending on the values of $\Delta\theta_o$. This is in stark contrast to the tank-treading RBC for which turning and crossing events were determined by ΔY_o only. As a result, critical separation $\Delta Y_{o,\mathrm{crit}}$ has a greater margin of uncertainty in tumbling RBC. The phase plot in the $\Delta\theta_o - \Delta Y_o$ plane for the tumbling RBC is shown in Fig. 6(*a*). A crossing event is observed for all values of $\Delta\theta_o$ if $\Delta Y_o \gtrsim 2.0\ \mu$m, and a turning event is observed if

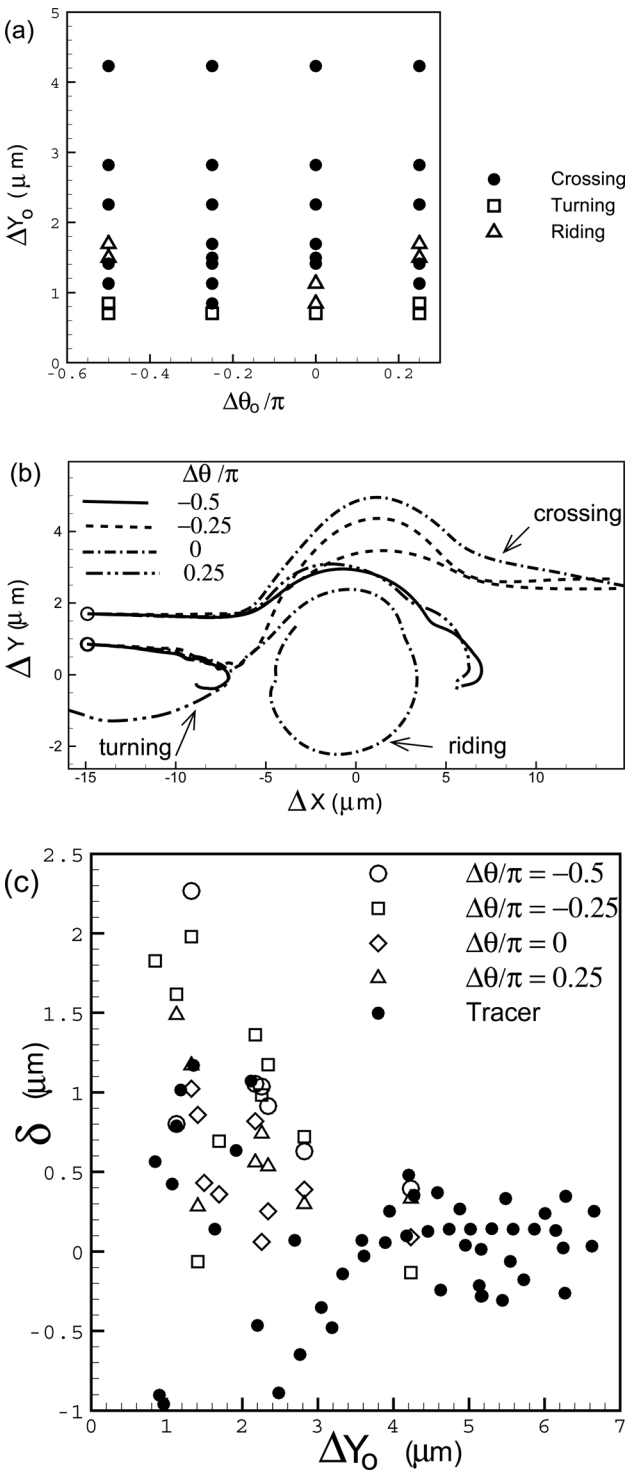

Fig. 6 Effect of initial relative orientation $\Delta\theta_o$ on turning, crossing, and riding events in presence of a tumbling RBC. (*a*) Phase plot in $\Delta\theta_o - \Delta Y_o$ plane. (*b*) sample trajectories obtained with different $\Delta\theta_o$ and ΔY_o. Turning, crossing, and riding trajectories are observed for the same ΔY_o at different $\Delta\theta_o$. (*c*) Platelet and tracer particle deflections δ in presence of a tumbling RBC.

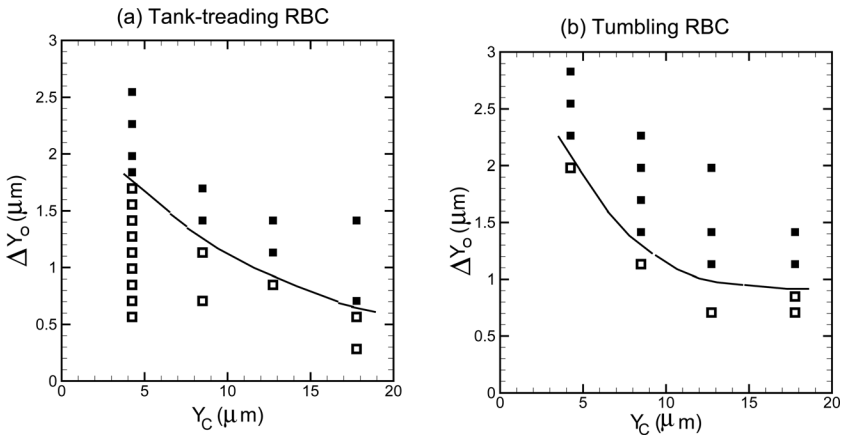

Fig. 7 Effect of wall proximity on turning and crossing events in presence of (*a*) tank treading and (*b*) tumbling RBC. The RBC/platelet interaction is simulated by releasing the RBC/platelet pair at various distances Y_C from the wall and for varying initial vertical separation ΔY_o. Open symbols indicate turning and filled symbols indicate crossing events.

$\Delta Y_o \lesssim 0.7\ \mu$m. But in the range $\Delta Y_o \sim 0.7 - 2.0\ \mu$m, all three types of interaction is possible depending on $\Delta\theta_o$. Two examples are shown in Fig. 6(*b*), where the platelet trajectory is plotted relative to the RBC for different values of $\Delta\theta_o$ but two fixed values of ΔY_o, 0.85 and 1.3 μm. For $\Delta Y_o = 0.85\ \mu$m, a crossing trajectory is observed when $\Delta\theta_o/\pi = -0.25$, a turning trajectory is observed when $\Delta\theta_o/\pi = -0.5$ and 0.25, and a riding trajectory is observed when $\Delta\theta_o/\pi = 0$. Second, in the crossing-type interaction, a wider variation in the post-interaction separation is observed in the tumbling RBC runs than that observed before in the tank-treading runs.

The deflection δ of the platelet trajectory for the crossing-type interactions in presence of the tumbling RBC is plotted in Fig. 6(*c*) as a function of ΔY_o for different $\Delta\theta_o$. While the general trend that δ decreases with increasing ΔY_o is observed, a significantly larger scatter in the data is evident here than that observed earlier for the tank-treading RBC due to the wider variation of the platelet trajectory. In some cases, δ is found to be negative when the post-interaction lateral separation is smaller than the initial separation. Also plotted are the deflection of the tracer particles which show even more scatter and larger negative values. Evidently, the tumbling RBC creates a greater mixing than the tank-treading RBC.

3.3 Near-Wall Interaction. Next we consider the effect of wall proximity on the RBC/platelet interaction. The pairwise interaction is simulated in the linear shear flow by releasing the RBC/platelet pair at different distances Y_C from one wall. The turning and crossing events are obtained from the simulations by varying the initial lateral separation ΔY_o. The results are shown in Fig. 7 as a function of Y_C and ΔY_o. This figure shows that the critical separation $\Delta Y_{o,\text{crit}}$ separating the crossing and turning events increases significantly near the wall with nearly a threefold increase from about 0.6 to 1.8 μm as Y_C is reduced from 18 to 4 μm in presence of the tank-treading RBC (Fig. 7(*a*)). This increase in $\Delta Y_{o,\text{crit}}$ is due to an increase in the lateral extent over which closed streamlines occur as the wall is approached. The increased $\Delta Y_{o,\text{crit}}$ near the wall suggests that the turning events have a higher probability to occur than the crossing events. We also observe that the deflection in the platelet trajectory due to the turning events is greater when it happens near the wall than away from the wall. It will be argued later that this increased $\Delta Y_{o,\text{crit}}$ provides a mechanism of continual platelet dispersal from the RBC-rich region of the vessel to the RBC-depleted plasma layer near the wall. The near-wall effect during a tumbling motion is presented in Fig. 7(*b*) which shows that $\Delta Y_{o,\text{crit}}$ is higher than that obtained for the tank-treading RBC.

When the RBC/platelet interaction occurs far away from a wall, the occurrence of the turning or crossing events depends only on the relative velocity between the RBC and the platelet, and hence, on the initial lateral separation ΔY_o, but not on the initial separation between the cells and the wall, Y_C or Y_{PLT}. One important consequence of the wall proximity is that the interaction depends not only on ΔY_o, but also on Y_C and Y_{PLT}. The results shown in Fig. 7 correspond to the scenario when the platelet is released further away from the wall than the RBC, i.e., $Y_{PLT} > Y_C$. We have also performed simulations when the platelets are released closer to the wall than the RBC, i.e., $Y_C > Y_{PLT}$. Figure 8 compares the platelet trajectories for these two configurations at three values of the lateral separation $|\Delta Y_o|$. Our simulations show that for the same value of $|\Delta Y_o|$ a turning event occurs when $Y_{PLT} > Y_C$, but a crossing event occurs when $Y_C > Y_{PLT}$. This result suggests that the value of the critical separation $\Delta Y_{o,\text{crit}}$ strongly depends on whether the RBC or the platelet is located closer to the wall. It also suggests that, near the wall, the turning events have a higher

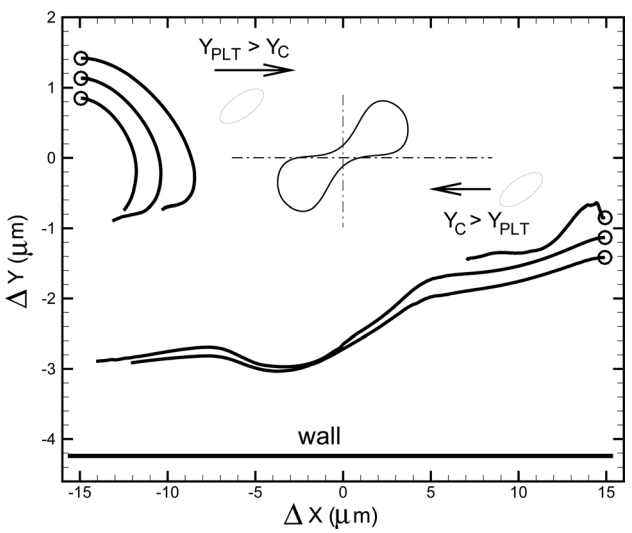

Fig. 8 Differential effect of wall proximity: For the same $|\Delta Y_o|$, a turning trajectory is observed when the platelet is located further away from the wall than the RBC ($Y_{PLT} > Y_C$), and a crossing trajectory is observed when the platelet is located closer to the wall ($Y_C > Y_{PLT}$)

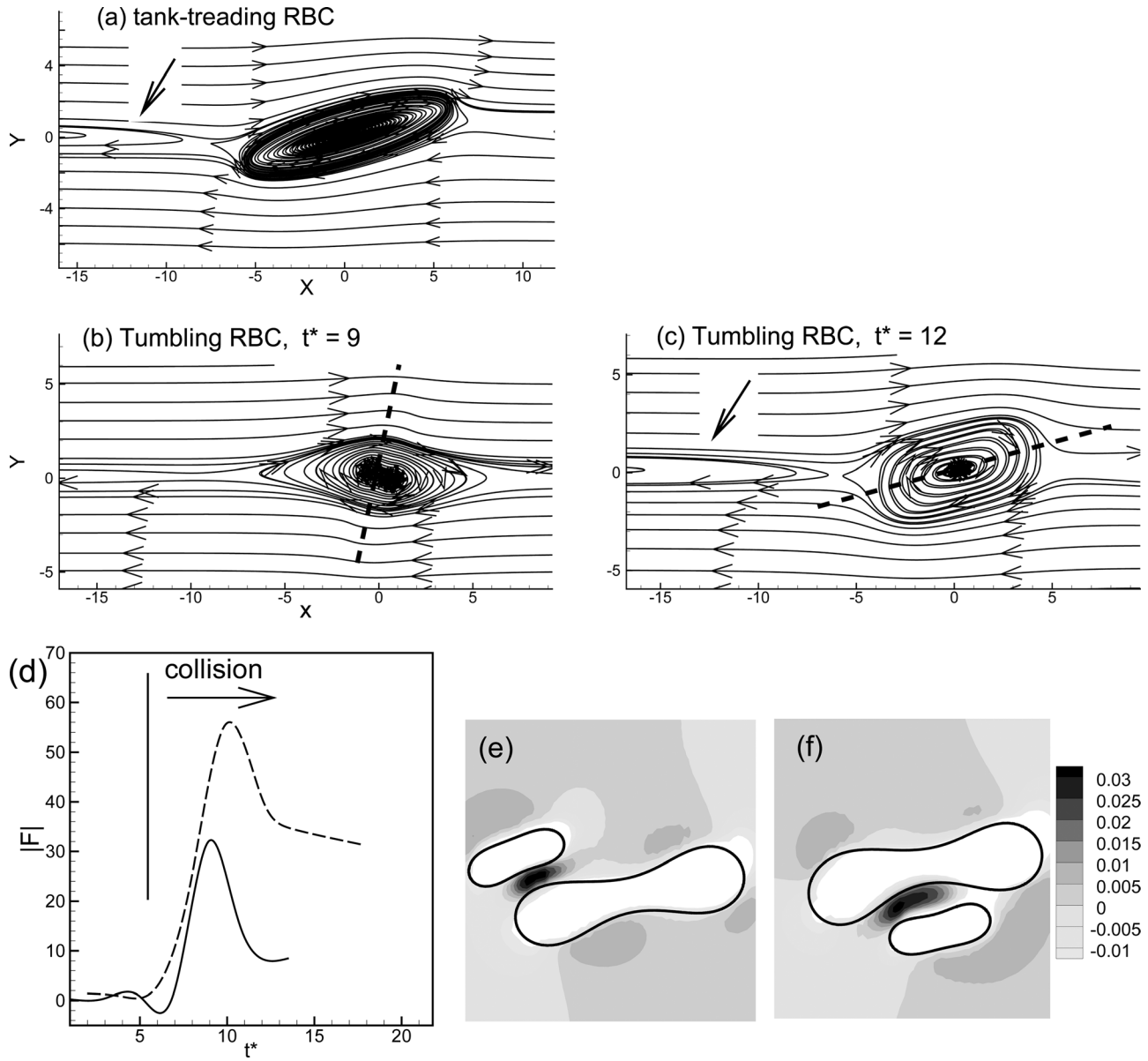

Fig. 9 (*a*)–(*c*) Streamlines around a tank-treading RBC (*a*), and a tumbling RBC [(*b*)and (*c*)] showing closed (indicated by the arrow) and open streamlines. The thick dash lines in (*b*) and (*c*) indicate the instantaneous alignment of the RBC major axis. (*d*) Spatially averaged force on the platelet as a function of time for a representative crossing (—) and rolling (- - - - -). (*e*) and (*f*) Contours of pressure for rolling at two time instances.

probability to occur when $Y_{PLT} > Y_C$, but the crossing events have a higher probability to occur when $Y_C > Y_{PLT}$.

3.4 Streamlines and Forces. The different types of interaction observed here can be partly explained by analyzing the streamlines around the RBC as shown in Figs. 9(*a*)–9(*c*). For the tank-treading case, the streamlines remain unchanged in time as the RBC motion is nearly steady. There is a critical lateral length y_o below which the streamlines turn around, and above which they extend from $-\infty$ to $+\infty$. The crossing event usually occurs when the platelet is released above this critical y_o, and a turning occurs when it is released below the critical y_o. It should however be mentioned that unlike a passive tracer, a platelet because of its finite size is not going to follow a streamline exactly. Unlike in the tank-treading case, the streamlines around a tumbling RBC are highly time dependent due to the changing orientation of the RBC. The closed streamlines are observed at some instants but not always. Hence the turning and crossing events in this case would depend on the instantaneous location and orientation of the platelet relative to those of the RBC. Furthermore, closed streamlines can exist in a narrow region around the RBC. If the platelet is trapped in this region, a riding trajectory would occur. The dynamic nature of the streamlines around a tumbling RBC leads to a more complex platelet trajectory than that observed in presence of a tank-treading RBC.

The forces acting on the platelet during different types of interactions are shown in Fig. 9(*d*). These forces are computed by spatially averaging the membrane forces over the cell surface. It may be noted that the there are only two types of forces that are experienced by the platelet/RBC: the hydrodynamic force, and the collision force. No other types of force (e.g., electrostatic repulsion, adhesion) are considered here. In case of turning behavior, the RBC/platelet do not come close to each other; so there is no collisional force. The platelet trajectory is entirely determined by the deflection of the streamlines due to the presence of the RBC as shown earlier. In this case, the force on the platelet is purely hydrodynamic. In case of crossing and rolling behaviors, the

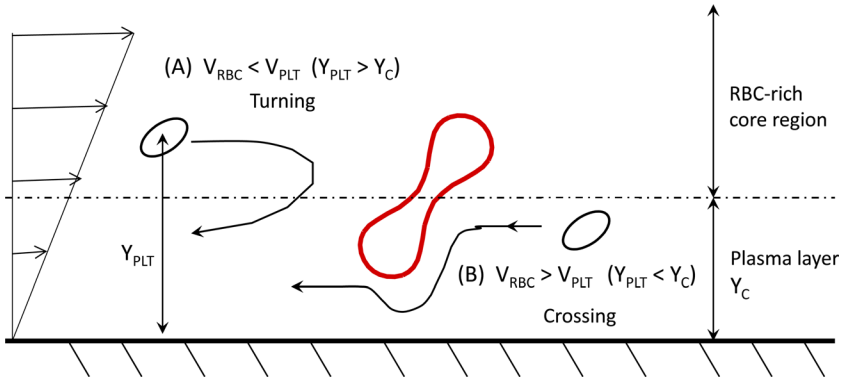

Fig. 10 A proposed mechanism of continuous platelet dispersal from the RBC-rich region of the vessel towards the wall based on the trajectory deflection by a succession of turning and crossing events occurring due to the interaction with a RBC flowing near the edge of the plasma layer. When the platelet is initially located farther away from the wall than the RBC, a turning event has the higher probability to occur (since $\Delta Y_{o,\mathrm{crit}}$ is large) that would bring the platelet from the RBC-rich region to the plasma layer [scenario (A) in the figure]. If a subsequent interaction occurs, a crossing event is likely to occur (since the platelet is now located closer to the wall than the RBC and $\Delta Y_{o,\mathrm{crit}}$ is small), bringing the platelet even closer to the wall [scenario (B)].

collisional force arises in form of the lubrication force (which is again hydrodynamic in nature) generated in the narrow gap between the RBC and the platelet. Our data shows that the force magnitude increases significantly during the encounter which implies that the collisional force is much higher than the hydrodynamic force. Our data further show that the force magnitude is much higher during the rolling interaction than the crossing interaction. This is because the platelet nearly sticks to the RBC for a longer time during the rolling interaction. In order to see the origin of these forces, we plot the contours of pressure in the shear plane for a rolling interaction in Figs. 9(*e*) and 9(*f*). This clearly shows that the pressure in the gap between the RBC and the platelet increases significantly during the close interaction leading to the lubrication force as the fluid is squeezed during the collision.

4 Discussion

In this article we presented three-dimensional numerical simulations of hydrodynamic interaction between a red blood cell and a platelet in a wall-bounded shear flow. The dynamics and large deformation of the RBC were fully resolved in the simulations. Instead of considering a suspension of multiple cells, we focused on an isolated RBC/platelet pair to quantify the influence of the tank treading and tumbling dynamics and the wall proximity on the deflection of individual platelet trajectory without the noise from other cells. Our results suggested the existence of two types of interaction. In a crossing-type interaction the platelet comes in close proximity to the RBC, rolls over it, and continues to move in the same direction. In a turning-type interaction, the platelet turns away before coming close to the RBC. The occurrence of any one of these events depends on the initial lateral separation ΔY_o between the platelet and RBC centers-of-mass. The crossing events occur when ΔY_o is above a critical separation $\Delta Y_{o,\mathrm{crit}}$, and the turning events occur when ΔY_o is below $\Delta Y_{o,\mathrm{crit}}$. Similar crossing and turning events have been observed during the interaction of two identical (homotypic) red blood cells and liquid drops in shear flow [37,57,58]. The present work deals with heterotypic particles.

The presence of a bounding wall is observed to have a significant influence on the crossing and turning events. When the RBC/platelet interaction occurs far away from a wall, the occurrence of the turning or crossing events depends only on the relative velocity between the RBC and the platelet as determined by their initial separation ΔY_o in a linear shear flow. In presence of a wall, the interaction depends not only on ΔY_o, but also on the lateral separation between the cells and the wall, Y_C and Y_{PLT}. When the RBC is released closer to the wall than the platelet, i.e., $Y_{PLT} > Y_C$, the critical separation $\Delta Y_{o,\mathrm{crit}}$ is observed to increase almost threefold. This result implies that the turning events have several-fold higher probability to occur than the crossing events when the RBC is flowing closer to the wall than the platelet. On the contrary, if the platelet is initially located closer to the wall than the RBC, i.e., $Y_{PLT} < Y_C$, the critical separation $\Delta Y_{o,\mathrm{crit}}$ was observed to be significantly lower, implying that the crossing events are more likely to occur in this scenario.

We now propose a mechanism of continuous platelet dispersal from the core of the vessel towards the wall based on the trajectory deflection. Consider the RBC flowing at the edge of the plasma layer as shown in Fig. 10. If a platelet is initially located in the RBC-rich region [scenario (A) as marked in the figure], i.e., $Y_{PLT} > Y_C$, a turning event is likely to occur (since $\Delta Y_{o,\mathrm{crit}}$ is large as found by the simulations and shown in Fig. 7), which will bring it in to the plasma layer. At this time, the platelet is located closer to the wall than the RBC (i.e., $Y_{PLT} < Y_C$). Now if another pairwise interaction occurs, that would likely result in a crossing event (since $\Delta Y_{o,\mathrm{crit}}$ is small), bringing the platelet even closer to the wall [scenario (B) as marked in the figure]. Our numerical trajectory in Fig. 8 showed that after the event (B) the platelet center-of-mass can be within 1 μm from the wall, giving it the opportunity to bind to the wall. Thus, the turning and crossing events, when they occur in succession as shown here, provide an effective mechanism to continually drive the platelets away from the RBC-rich region of the vessel in to the RBC-depleted plasma layer and further towards the wall.

The influence of RBC deformation and the finite cell size is most noticeable in the computed lateral deflection δ which can be considered as an indirect measure of the platelet drift due to the crossing events. While δ is generally observed to decrease with increasing initial RBC/platelet separation ΔY_o, it shows a pronounced local minimum at $\Delta Y_o \sim 1.3 - 1.8\,\mu$m. This nonmonotonic trend of δ is due to the deformation of the RBC caused by the platelet upon collision. We showed that the local minimum in δ is accompanied with an increase in the RBC deformation index. The finding that a platelet can impart a considerable deformation to the RBC underscores the importance of considering the finite size of the platelet in any theoretical model of platelet drift [25,26]. It also has other biological implication as RBC deformation was shown to increase ATP release [59], and the presence of

ADP is known to initiate platelet aggregation [10]. Additionally, the nonmonotonic trend of δ is not observed for deformable sphere-sphere collision, and for tracer particle deflection. The platelet deflection is generally observed to be higher than the tracer deflection, except near the local minimum, and is likely caused by an increased volume exclusion due to the finite platelet size.

The different dynamics of the RBC, i.e., the tank treading and the tumbling motion, are observed to cause considerable differences in the platelet motion. Most notably, the critical lateral separation $\Delta Y_{o,\mathrm{crit}}$ is found to be higher for the tumbling RBC. This finding is important as the tank-treading motion occurs at relatively high shear rates, while the tumbling motion occurs at low shear rates. The tumbling motion can also occur due to the loss of deformability caused by various pathological conditions of the RBC, which is believed to be associated with higher risk of thrombogenesis [60].

Another important result is the wide variability of the platelet trajectory observed over the range of initial inclination and lateral separation that is absent in the deformable sphere-sphere interaction. For the deformable sphere-sphere interaction, a crossing event always leads to an increased lateral separation, and a monotonic change in ΔY_o leads to a monotonic change in the post-interaction separation. In contrast, such a monotonic change is not observed for the RBC/platelet interaction. In some simulations, we observed that the post-interaction separation was less than the initial separation leading to a negative value of δ, in a stark contrast to the sphere-sphere collision. This result not only underscores the importance of incorporating the effect of the nonspherical shapes and finite size of the RBC and platelet in any drift model [25,26], it also suggests that the shear-induced diffusion process in the RBC/platelet suspension is more complex than that in a spherical particle suspension. The variability of the platelet trajectory is observed to increase significantly when the tumbling RBC is considered resulting in a larger scatter in δ. This result is in qualitative agreement with the experimental observation that the platelet diffusivity increases with decreasing RBC deformability [18].

The numerical data can be used to make an approximate estimate of the enhanced platelet diffusion coefficient in presence of the RBCs. Taking the value of δ to be $\sim 1\ \mu$m from Fig. 5(*a*), a shear rate in the range of 100–1000 s^{-1} for which a normal red blood cell would be tank treading, and the interaction time of $t \sim 0.01 - 0.1$ s obtained from the simulations (corresponding to a dimensionless time of $t^* \sim 10$), we find a diffusion coefficient $D_{\mathrm{eff}} \sim \delta^2/t = 10^{-6} - 10^{-7}$ cm^2/s. Although this is a simple estimate, and is based on a single cells rather than an actual suspension, this value is surprisingly similar to the ones reported in experiments [21–23], and computer simulations with multicellular suspension [34], and nearly 2 to 3 orders of magnitude higher than the Brownian diffusion coefficient of $\sim 10^{-9}$ cm^2/s [61].

In conclusion, we have presented three-dimensional numerical simulation of hydrodynamic interaction between a platelet and an erythrocyte by fully resolving the deformation and dynamics of the cells. We observed a wide variability in the platelet trajectory under the influence of the tank treading and tumbling motion of the erythrocyte, and proposed a mechanism of continual platelet removal from the core of a vessel towards the plasma layer. While the realistic blood flow is a dense suspension, and the platelet drift is the result of the multicellular interaction, understanding the two-body interaction as presented here is a first step before addressing the more complex problem of platelet drift in whole blood. The present work shows that even the two-body interaction could be quite complex due to the nonspherical cellular shape, erythrocyte deformation, and tank treading and tumbling motion. Nevertheless, the numerical methodology could be readily extended to consider multiple cells as done in our previous publications [43], and hence to study the mechanism of platelet drift in a suspension. It can be equipped with platelet adhesion dynamics [38,39] to study the effect of the flowing red blood cells on the adhesion and detachment of platelets to and from the wall, and hence the development of microthrombi. The immersed-boundary method also allows us to study these phenomena in more complex geometry such as stenosis.

Acknowledgment

K.V. and P.B. acknowledge support through a subcontract from University of Pennsylvania. S.L.D acknowledges support from National Institutes of Health through a Grant No. NIH R01 HL103419. Computational support from NSF-supported Teragrid resources at TACC and NCSA is acknowledged.

References

[1] Flamm, M. H., and Diamond, S. L., 2012, "Multiscale Systems Biology and Physics of Thrombosis Under Flow," Ann. Biomed. Eng., **11**, p. 2355.
[2] Ruggeri, Z. M., and Mendolicchio, G. L., 2007, "Adhesion Mechanisms in Platelet Function," Circ. Res., **100**, pp. 1673–1685.
[3] Wootton, D. M., and Ku, D. N., 1999, "Fluid Mechanics of Vascular Systems, Diseases, and Thrombosis," Ann. Rev. Biomed. Eng., **1**, pp. 299–329.
[4] Xu, C., and Wootton, D. M., 2004, "Platelet Near-Wall Excess in Porcine Whole Blood in Artery-Sized Tubes Under Steady and Pulsatile Flow Conditions," Biorheology, **41**, pp. 113–125.
[5] Yeh, C., and Eckstein, E. C., 1994, "Transient Lateral Transport of Platelet-Sized Particles in Flowing Blood Suspensions," Biophys. J., **66**, pp. 1706–1716.
[6] Uijttewaal, W. S., Nijhof, E. J., Bronkhorst, P. J., Den Hartog, E., and Heethaar, R. M., 1993, "Near-Wall Excess of Platelets Induced by Lateral Migration of Erythrocytes in Flowing Blood," Am. J. Physiol. Heart, **264**, pp. H1239–H1244.
[7] Koleski, J. F., and Eckstein, E. C., 1991, "Near Wall Concentration Profiles of 1.0 and 2.5 μm Beads During Flow of Blood Suspensions," Trans. Am. Soc. Artif. Intern. Organs, **37**, pp. 9–12.
[8] Eckstein, E. C., Koleski, J. F., and Waters, C. M., 1989, "Concentration Profiles of 1.0 and 2.5 μm Beads During Blood Flow. Hematocrit Effects," Trans. Am. Soc. Artif. Intern. Organs, **35**, pp. 188–190.
[9] Aarts, P. A., van den Broek, S. A., Prins, G. W., Kuiken, G. D., Sixma, J. J., and Heethaar, R. M., 1988, "Blood Platelets Are Concentrated Near the Wall and Red Blood Cells, in the Center in Flowing Blood," Arteriosclerosis, **8**, pp. 819–824.
[10] Tilles, A. W., and Eckstein, E. C., 1987, "The Near-Wall Excess of Platelet-Sized Particles in Blood Flow: Its Dependence on Hematocrit and Wall Shear Rate," Microvasc. Res., **33**, pp. 211–223.
[11] Tangelder, G. J., Teirlinck, H. C., Slaaf, D. W., and Reneman, R. S., 1985, "Distribution of Blood Platelets Flowing in Arterioles," Am. J. Physiol., **248**(3 Pt 2), pp. H318–H323.
[12] Turitto, V. T., and Hall, C. L., 1998, "Mechanical Factors Affecting Hemostasis and Thrombosis," Thromb. Res., **92**(Suppl2), pp. S25–S31.
[13] Goldsmith, H. L., Bell, D. N., Braovac, S., Steinberg, A., and McIntosh, F., 1995, "Physical and Chemical Effects of Red Cells in the Shear-Induced Aggregation of Human Platelets," Biophys. J., **69**, pp. 1584–1595.
[14] Turitto, V. T., and Weiss, H. J., 1983, "Platelet and Red Cell Involvement in Mural Thrombogenesis," Ann. N.Y. Acad. Sci., **416**, pp. 363–376.
[15] Turitto, V. T., and Weiss, H. J., 1980, "Red Blood Cells: Their Dual Role in Thrombus Formation," Science, **207**, pp. 541–543.
[16] Turitto, V. T., and Baumgartner, H. R., 1975, "Platelet Interaction With Subendothelium in a Perfusion System: Physical Role of Red Blood Cells," Microvasc. Res., **9**, pp. 335–344.
[17] Eckstein, E. C., Blisker, D. L., Waters, C. M., Kippenhan, J. S., and Tilles, A. W., 1987, "Transport of Platelets in Flowing Blood," Ann. N.Y. Acad. Sci., **516**, pp. 442–452.
[18] Aarts, P. A. M. M., Heethaar, R. M., and Sixma, J. J., 1984, "Red Blood Cell Deformability Influences Platelets-Vessel Wall Interaction in Flowing Blood," Blood, **64**(6), pp. 1228–1233.
[19] Goldsmith, H. L., 1971, "Red Cell Motions and Wall Interactions in Tube Flow," Fed. Proc. **30**(5), pp. 1578–1590.
[20] Eckstein, E. C., and Belgacem, F., 1991, "Model of Platelet Transport in Flowing Blood With Drift and Diffusion Terms," Biophys. J., **60**, pp. 53–69.
[21] Turitto, V. T., Benis, A. M., and Leonard, E. F., 1972, "Platelet Diffusion in Flowing Blood," Ind. Eng. Chem. Fundam., **11**, pp. 216–223.
[22] Antonini, G., Guiffant, G., Quemada, D., and Dosne, A. M., 1978, "Estimation of Platelet Diffusivity in Flowing Blood," Biorheology, **15**, pp. 111–117.
[23] Diller, T. E., 1988, "Comparison of Red Cell Augmented Diffusion and Platelet Transport," J. Biomech. Eng., **110**, pp. 161–163.
[24] Kim, S. P., Ong, K., Yalcin, O., Intaglietta, M., and Johnson, P. C., 2009, "The Cell-Free Layer in Microvascular Blood Flow," Biorheology, **46**, pp. 181–189.
[25] Tokarev, A. A., Butylin, A. A., Ermakova, E. A., Shnol, E. E., Panasenko, G. P., and Ataullakhanov, F. I., 2011, "Finite Platelet Size Could Be Responsible for Platelet Margination Effect," Biophys. J., **101**, pp. 1835–1843.
[26] Tokarev, A. A., Butylin, A. A., and Ataullakhanov, F. I., 2011, "Platelet Adhesion From Shear Blood Flow Is Controlled by Near-Wall Rebounding Collisions With Erythrocytes," Biophys. J., **100**, pp. 799–808.

[27] Fischer, T. M., Stohr-Liesen, M., and Schmid-Schonbein, H., 1978, "The Red Cell As a Fluid Droplet: Tank-Tread Like Motion of the Human Erythrocyte Membrane in Shear Flow," Science, **202**, p. 894.
[28] Keller, S. R., and Skalak, R., 1982, "Motion of a Tank-Treading Ellipsoidal Particle in a Shear Flow," J. Fluid Mech., **120**, pp. 27–47.
[29] Abkarian, M., Faivre, M., and Viallat, A., 2007, "Swinging of Red Blood Cells Under Shear Flow," Phys. Rev. Lett., **98**, p. 188302.
[30] Skotheim, J. M., and Secomb, T. W., 2007, "Oscillatory Dynamics and the Tank-Treading-to-Tumbling Transition," Phys. Rev. Lett., **98**, p. 078301.
[31] Sui, Y., Chew, Y. T., Roy, P.Cheng, Y. P., and Low, H. T., 2008, "Dynamic Motion of Red Blood Cells in Simple Shear Flow," Phys. Fluids, **20**, p. 112106.
[32] AlMomani, T. H., Udaykumar, S., Marshall, J. S., and Chandran. K. B., 2008, "Micro-Scale Dynamic Simulation of Erythrocyte-Platelet Interaction in Blood Flow," Ann. Biomed. Eng., **36**, pp. 905–920.
[33] Crowl, L. M., and Fogelson, A. L., 2010, "Computational Model of Whole Blood Exhibiting Lateral Platelet Motion Induced by Red Blood Cells," Int. J. Numer. Methods Biomed. Eng., **26**, pp. 471–487.
[34] Crowl, L. M., and Fogelson, A. L., 2011, "Analysis of Mechanisms for Platelet Near-Wall Excess Under Arterial Blood Flow Conditions," J. Fluid Mech., **676**, pp. 348–375.
[35] Zhao, H., and Shaqfeh, E. S. G., 2011, "Shear-Induced Platelet Margination in a Microchannel," Phys. Rev. E, **83**, p. 061924.
[36] Zhao, H. E., Shaqfeh, S. G., and Narsimhan, V., 2012, "Shear-Induced Particle Migration and Margination in a Cellular Suspension," Phys. Fluids, **24**, p. 011902.
[37] Le, D.-V., and Chiam, K.-H., 2011, "Hydrodynamic Interaction Between Two Nonspherical Capsules in Shear Flow," Phys. Rev. E, **84**, p. 056322.
[38] Mody, N. A., and King, M. R., 2008, "Platelet Adhesive Dynamics. Part I: Characterization of Platelet Hydrodynamic Collisions and Wall Effects," Biophys. J., **95**, pp. 2539–2555.
[39] Mody, N. A., and King, M. R., 2008, "Platelet Adhesive Dynamics. Part II: High Shear-Induced Transient Aggregation Via GPIba-vWF-GPIba Bridging," Biophys. J., **95**, pp. 2556–2574.
[40] Peskin, C., 2002, "The Immersed Boundary Method," Acta Numerica, **11**, pp. 1–39.
[41] Tryggvason, G., Bunner, B., Esmaeeli, A., Al Rawahi, N., Tauber, W., Han, J., Nas, S., and Jan, Y., 2001, "A Front–Tracking Method for the Computations of Multiphase Flow," J. Comput. Phys., **169**, pp. 708–759.
[42] Doddi, S. K., and Bagchi, P., 2008, "Lateral Migration of a Capsule in a Plane Poiseuille Flow in a Channel" Int. J. Multiphase Flow, **34**, pp. 966–986.
[43] Doddi, S. K., and Bagchi, P., 2009, "Three-Dimensional Computational Modeling of Multiple Deformable Cells Flowing in Microvessels" Phys. Rev. E, **79**, p. 046318.
[44] Yazdani, A., and Bagchi, P., 2012, "Three-Dimensional Numerical Simulation of Vesicle Dynamics Using a Front-Tracking Method," Phys. Rev. E, **85**, p. 056308.
[45] Fung, Y. C., 1993, '*Biomechanics: Mechanical Properties of Living Tissues*, Springer, New York.
[46] Skalak, R., Tozeren, A., Zarda, P. R., and Chien, S., 1973, "Strain Energy Function of Red Blood Cell Membrane," Biophys. J., **13**, p. 245.
[47] Helfrich, W., 1973, "Elastic Properties of Lipid Bilayers: Theory and Possible Experiments," Z. Naturforsch. Teil C, **28**(11), pp. 693–703.
[48] Zhong-can, O.-Y., and Helfrich, W., 1989, "Bending Energy of Vesicle Membranes: General Expressions for the First, Second, and Third Variation of the Shape Energy and Applications to Spheres and Cylinders," Phys. Rev. A, **39**, pp. 5280–5288.
[49] Shrivastava, S., and Tang, J., 1993, "Large Deformation Finite Element Analysis of Non-Linear Viscoelastic Membranes With Reference to Thermoforming," J. Strain Anal., **28**, p. 31.
[50] Yazdani, A. Z. K., and Bagchi, P., 2011, "Phase Diagram and Breathing Dynamics of a Single Red Blood Cell and a Biconcave Capsule in Dilute Shear Flow," Phys. Rev. E, **84**, p. 026314.
[51] Fischer, T., and Schmid-Schonbein, H., 1977, "Tank Tread Motion of Red Cell Membranes in Viscometric Flow: Behavior of Intracellular and Extracellular Markers (With Film)," Blood Cells, **3**, pp. 351–365.
[52] Fischer, T. A., 1978, "Comparison of the Flow Behavior of Disc Shaped Versus Elliptic Red Blood Cells (RBC)," Blood Cells, **4**, pp. 453–461.
[53] Secomb, T. W., Hsu, R., and Pries, A. R., 1998, "A Model for Red Blood Cell Motion in Glycocalyx-Lined Capillaries," Am. J. Physiol., **274**, pp. H1016–H1022.
[54] Jeffery, G. B., 1922, "The Motion of Ellipsoidal Particles Immersed in a Viscous Fluid," Proc. R. Soc. London Ser. A, **102**, pp. 161–170.
[55] Lac, E., Morel, A., and Barthes-Biesel, D., 2007, "Hydrodynamic Interaction Between Two Identical Capsules in Simple Shear Flow," J. Fluid Mech., **573**, pp. 149–169.
[56] Loewenberg, M., and Hinch, E. J., 1997, "Collision of Two Deformable Drops in Shear Flow," J. Fluid Mech., **338**, pp. 299–315.
[57] Zurita-Gotor, M., Blawzdziewicz, J., and Wajnryb, E., 2007, "Swapping Trajectories: A New Wall-Induced Cross-Streamline Particle Migration Mechanism in a Dilute Suspension of Spheres," J. Fluid Mech., **592**, pp. 447–469.
[58] Li, X., and Sarkar, K., 2009, "Pairwise Interactions Between Deformable Drops in Free Shear at Finite Inertia," Phys. Fluids, **21**, p. 063302.
[59] Forsyth, A. M., Wan, J., Owrutsky, P. D., Abkarian, M., and Stone, H. A., 2011, "Multiscale Approach to Link Red Blood Cell Dynamics, Shear Viscosity, and ATP Release," Proc Natl. Acad. Sci. U.S.A., **108**, pp. 10986–10991.
[60] Leone, G., Sica, S., Chiusolo, P., Teofili, L., and De Stefano, V., 2001, "Blood Cell Diseases and Thrombosis," Haematologic, **86**, pp. 1236–1244.
[61] Goldsmith, H. L., and Turitto, V. T., 1986, "Rheological Aspects of Thrombosis and Hemostasis: Basic Principles and Applications. ICTH-Report 781 Subcommittee on Rheology of the International Committee on Thrombosis and 782 Hemostasis," Thromb. Haemost., **55**(3), pp. 415–435.